JOURNAL OF CATALYSIS 145, 335–343 (1994)

Catalytic NH_3 Decomposition by Topotactic Molybdenum Oxides and Nitrides: Effect on Temperature Programmed γ-Mo_2N Synthesis

R. S. Wise and E. J. Markel[1]

Department of Chemical Engineering, University of South Carolina, Columbia, South Carolina 29208

Received January 4, 1993; revised September 8, 1993

The extent of NH_3 decomposition during temperature-programmed synthesis of high surface area γ-Mo_2N from MoO_3 is reported. It was found that the flowing NH_3 feed gas is up to 99.88% decomposed at the elevated temperatures of the synthesis reaction. Kinetic data were used in a two-dimensional coupled heat and mass transfer model of the reactor to calculate bed temperatures from measured furnance temperature data. At the highest reaction temperatures, the endothermic NH_3 decomposition reaction strongly affects the bed temperatures, even in the small (0.1 g) bed used in the kinetic study. Local temperature ramps twice as high as the furnace ramping rate were found. Models of large reactant beds show that scale-up of the NH_3/MoO_3 reaction is difficult because of hindered heat transfer. It is proposed that N_2/H_2 mixtures be used in large-scale syntheses of topotactic γ-Mo_2N to reduce heat transfer problems.

INTRODUCTION

The production of high specific surface area (up to 220 m^2/g) γ-Mo_2N by temperature programmed reaction of MoO_3 and flowing NH_3 has been reported by earlier investigators (1, 2). These materials are particularly promising for heterogeneous catalysis because in contrast to supported catalysts in which a portion of the available surface area is due to the inactive support, all of this catalyst's surface area is due to the active material. In addition, it is possible to manipulate the solid phase chemistry, replacing nitrogen in the metal lattice to form high surface area molybdenum carbides, borides, and hydrides (1, 3). High specific surface area γ-Mo_2N has been studied as a catalyst for NH_3 synthesis (4), ethane hydrolysis (5), CO hydrogenation (6), hydrodenitrogenation (6, 7), and hydrodesulfurization (2).

The known Mo_2N synthesis reaction requires a slow temperature ramp to 980 K and a high NH_3 space velocity through a packed bed of powdered MoO_3 to produce very high surface areas (1, 2). Reduced space velocities, increased reactant particle sizes, and faster temperature ramping rates lead to reduced specific surface areas. The mechanism by which these macroscopic reaction variables influence the synthesis reaction and product nanostructure is the subject of this work. We have previously found (8) that these reaction conditions result in elevated water concentrations in the flow reactor, leading to lower surface areas by hydrothermal sintering or lattice fluidization. It has also been postulated that depletion of NH_3 by catalytic or noncatalytic decomposition may influence the reaction mechanism by altering the reaction chemistry. Previous studies have shown that NH_3 is completely decomposed in NH_3/MoO_3 reactions used to produce large amounts (ca. 50 g) of moderate surface area Mo_2N (3).

The purpose of this work is to quantify the extent of NH_3 decomposition during the synthesis of high surface area Mo_2N and to investigate the effect of NH_3 decomposition of Mo_2N synthesis and surface area generation. Changes in gas/solid reaction chemistry as NH_3 decomposes to N_2 and H_2 and the effect of the endothermic decomposition reaction on bed temperatures are of particular interest. It is shown that while altered gas composition is not detrimental (8, 9) to achieving high surface area, the effect of NH_3 decomposition on bed temperatures is significant.

REVIEW

Kinetics

The NH_3 synthesis and decomposition reactions have been topics of study for over 90 years, providing fertile ground for the development of many fundamental principles of kinetics and catalysis (10–12). Both reactions have been studied over pressures ranging from high vacuum to hundreds of atmospheres (commercial synthesis conditions) and using a range of catalysts. At the temperatures and pressures used in this study (600–1000 K, ~1 atm),

[1] To whom correspondence should be addressed.

0021-9517/94 $6.00

experimental data for NH_3 decomposition on molybdenum, tungsten, iron, and platinum (13–16) are reasonably fitted by

$$r = k' P_{NH_3}^m \quad [1a]$$

or

$$r = kP_{NH_3}/(1 + KP_{NH_3}), \quad [1b]$$

where k, k', K and m ($0 \leq m \leq 1$) are constants. The reaction is generally zero order in N_2 and H_2, first order in NH_3, and can be inhibited by NH_3. However, while the kinetic expression is of the form of a Langmuir–Hinshelwood mechanism, the reaction rate is determined by adsorption/desorption phenomena and can be described by the Tamaru mechanism (17),

$$NH_3 + * \rightarrow \text{immaterial} \quad [2a]$$

$$*N_2 \rightarrow N_2 + *, \quad [2b]$$

in which dissociative NH_3 adsorption and dinitrogen desorption reactions are not at equilibrium and thereby they determine the overall rate of reaction by controlling the dynamic balance of supply and desorption of chemisorbed nitrogen. At lower temperatures, dissociative NH_3 adsorption is at equilibrium and the overall decomposition reaction obeys the Temkin–Pyzhev mechanism (18),

$$NH_3 + * \leftrightarrow N^* + \tfrac{3}{2} H_2 \quad [3a]$$

$$*N_2 \rightarrow N_2 + * \quad [3b]$$

$$r = k(P_{NH_3}^2/P_{H_2}^3/)^\alpha, \quad [3c]$$

where k and α are constants and the reaction rate is determined by the rate of dinitrogen desorption. In the Temkin–Pyzhev mechanism the rate of ammonia decomposition is strongly retarded by the presence of hydrogen while the rate expression of the Tamaru mechanism is independent of hydrogen. Tamaru provides a theoretical basis for calculating the temperature of transition from the Temkin–Pyzhev to the Tamaru mechanism (17) which indicates that the Tamaru mechanism will prevail at high temperatures (above 1000 K) and low hydrogen partial pressures,

$$T_{\text{transit}} = \frac{E_d^N - E_d^A}{R \ln(k_{do}^N/(k_{do}^A P_{H_2}))}, \quad [4]$$

where E_d^N and E_d^A are the activation energies for desorption of nitrogen and ammonia, respectively. Similarly, k_{do}^N and k_{do}^A are the preexponential factors of the rate constant for the nitrogen and ammonia desorption steps. Experimentally determined transition temperatures (13–16, 19) are lower than those predicted by theory.

EXPERIMENTAL

Synthesis Reactions

All temperature programmed reactions were performed using 4 mm ID × 8 mm OD × 1 m ID quartz tubular flow reactors fitted with porous 10 mm quartz frits. Each reactor was loaded with 0.1 g MoO_3 powder (Johnson Matthey, 99.99%) and connected to an NH_3 source (Matheson, 99.9995%). NH_3 flow was metered using a variable area rotameter upstream of the reactant bed. A 100 centimeter Lindberg furnace equipped with a programmable temperature controller was used for all temperature-programmed reactions. The thermocouple was located outside the quartz tube in the furnace air. A thermocouple well in the reacting solid bed was not used for two reasons: (1) the thermocouple well would interfere excessively with gas flow and heat transfer in the tiny reactant bed and (2) the bed is not isothermal, leading to the experimental difficulties of placing a thermocouple reliably in a given location (both axially and radially) in a tiny bed with large temperature gradients.

Each synthesis reaction began with a brief period for stabilization of the gas flow, followed by initiation of the temperature ramping program. When the temperature program was complete, gas flow was maintained as the reaction vessel was removed from the furnace. Most of the high surface area materials were air sensitive and oxidize completely if exposed to air immediately following reaction. Air stable samples were formed using a passivation procedure (2) in which air is allowed to slowly diffuse though 0.5 m by 1 cm ID tubing to the sample over a period of 24. This procedure was selected to minimize over-oxidation of the sample: assuming that mass transfer of air occurs only by diffusion and that any oxygen present reacts immediately with the solid surface, only 2–3 monolayers of oxygen can form on the surface during the passivation procedure, depending on the type of metal oxide surface structure assumed. We have previously shown (20) that passivated γ-Mo_2N is stabilized by an amorphous oxide surface layer with an infrared spectrum like that of MoO_2 and a slow rate of passivation is required due to the exothermic nature of the oxidation. Other reported passivation methods (1–7) involve flowing inert gases containing 1% oxygen—much higher oxygen levels than used in our procedure. Regardless of the method used, it is clear when a sample is not properly passivated: the sample burns brightly when exposed to air.

The composition of the reactor effluent during temperature programmed reaction was determined by gas chromatography. Gas samples were automatically injected by

a pneumatically actuated sampling valve on the reactor effluent line. Samples were sent to a Hewlett Packard 5890A gas chromatograph equipped with a thermal conductivity detector (TCD) and fitted with two columns. A 2 m by $\frac{1}{8}$ in. diameter stainless steel Porapak N (AllTech Associates) column was used for quantitative separation of H_2O and NH_3, while a 6 m by $\frac{1}{8}$ in. diameter stainless steel silica gel column was used for quantitative determination of N_2. All columns employed helium (Matheson, 99.9995%) as the carrier gas. Automatic gas sampling and data acquisition were controlled by an IBM PC/AT computer equipped with an Interactive Microwave A/D converter, logic board, and software. Samples for NH_3/H_2O separation were taken every 780 sec. Samples for N_2 determination were taken every 240 sec.

Characterization

Solid products were analyzed using a Rigaku X-ray diffractometer (model D-max B) equipped with a Cu source and a grating monochromator system for rejection of spurious lines. Samples were ground as required and mounted on backless aluminum sample holders using an amorphous adhesive tape. All data were compared to JCPDS catalogue values (21) for identification.

X-ray diffraction peak widths were used to determine the size of coherently diffracting crystalline domains in solid products using the Scherrer equation (22),

$$d_{hkl} = K\lambda/b \cos\theta \qquad [5]$$

where b is the corrected peak width at half maximum in terms of goniometer angle 2θ, λ is the incident radiation wavelength, θ is the angle of diffraction, d_{hkl} is the dimension of coherently reflecting domains in the $\langle hkl \rangle$ direction, and K is taken as unity. The corrected value b should be distinguished from B, the measured angular width at half maximum (FWHM). The value of b is obtained using Warren's formula for Gaussian type curves, $b^2 = B^2 - b_0^2$, where b_0 is the FWHM interpolated to the angle of interest of KBr or a similar material with particle dimensions in excess of 3000 Å (22). It should also be mentioned that the value of d_{hkl} is used as a relative measure of lattice extent in the $\langle hkl \rangle$ direction only. If d is defined as the cube root of volume, the value of K would be a function of the crystallite morphology and orientation. The solid particle diameter may also be estimated from surface area using the relation $S_g = 6/\rho d_p$ (1).

BET surface area analysis and pore volume measurements were performed using a Micromeritics 2700 dynamic adsorption analyzer. The N_2/He mixtures used in adsorption measurements were prepared in the laboratory by mixing commercial gases (Matheson N_2, 99.9995%, and He, 99.9995%) in a Sierra electronic dual channel mass flow controller. An integrating thermal conductivity detector was used to determine test gas composition during adsorption/desorption. Adsorption was carried out at 77 K.

RESULTS

NH_3 Decomposition

Decomposition of NH_3 during temperature programmed reaction of MoO_3 and NH_3 was monitored by gas chromatographic analyses of the reactor effluent for NH_3 and N_2 (Figure 1). An NH_3 flow rate of 170,000 hr^{-1} and a temperature ramping rate of 0.6 K/min from 300 K to the final reaction temperature of 980 K were used. In this range of temperatures, only N_2, H_2, NH_3, and H_2O were observed in the effluent. No gas-phase reaction intermediates were observed. At the final reaction temperature of 980 K, decomposition is nearly complete: only 1250 ppm NH_3 remains. Analyses for N_2 were much more accurate than those for NH_3 because the N_2 peaks were much narrower and did not overlap significantly with other peaks. All kinetic calculations were, therefore, based on N_2 analyses.

The H_2O observed in the reactor effluent is a product of the gas/solid reaction. It was not possible to reliably separate H_2O and NH_3 from mixtures containing more than 1% NH_3. H_2O concentrations as high as 700 ppm were observed at the final reaction temperature, indicating that the gas/solid reaction was still underway when 980 K was reached. For this reason, reaction was allowed to

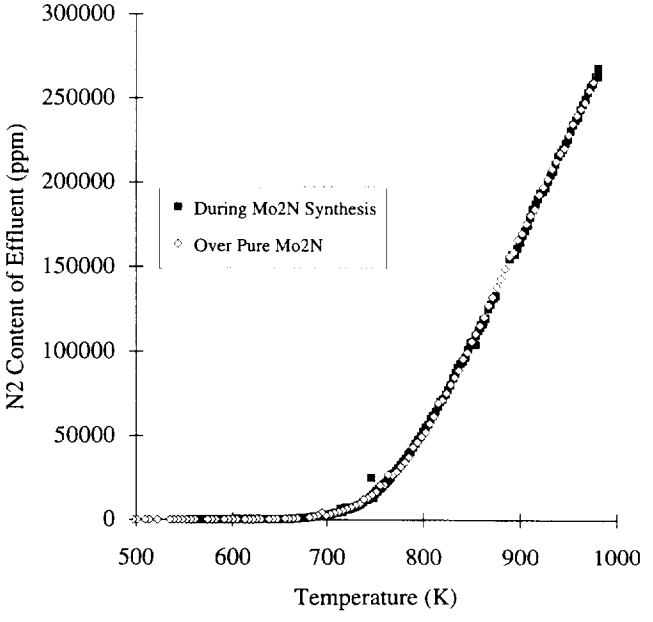

FIG. 1. N_2 content of synthesis reaction effluent.

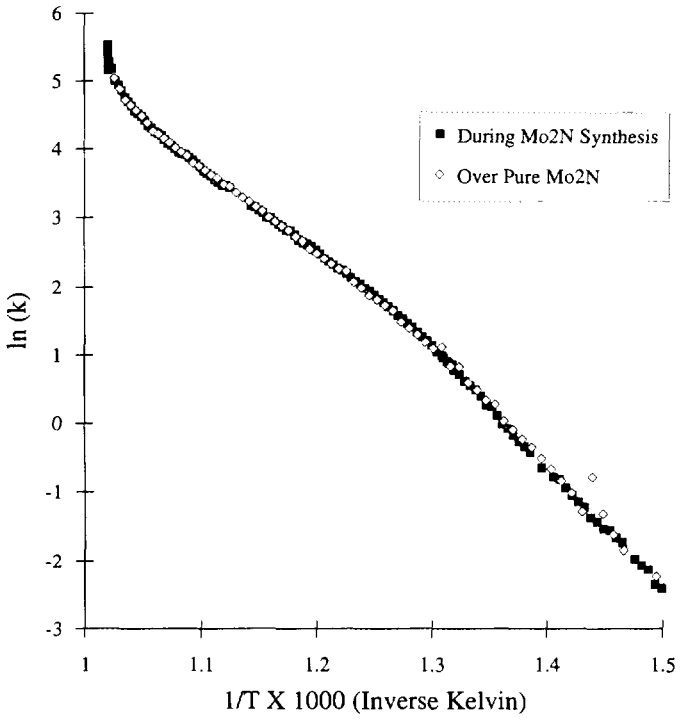

FIG. 2. Arrhenius plot for NH_3 decomposition reaction, first order kinetics. Inverse furnace temperature is shown on the horizontal axis. Deviations from linearity at high temperature are due to differences between furnace and catalyst bed temperatures.

continue for 2 hr at 980 K to ensure complete conversion of MoO_3 to Mo_2N.

The extent of NH_3 decomposition over pure, unpassivated Mo_2N was also examined, based on chromatograph analyses for N_2 formation. The N_2 content of the reactor effluent (Fig. 1) was found to correspond closely to that observed during Mo_2N syntheses over a wide range of temperatures. Small but measurable differences were observed at intermediate temperatures where nitrogen is consumed by nitride formation reactions. The fractional conversion of NH_3 was virtually independent of the solid composition.

The NH_3 decomposition experiments were repeated using reactors with 2 mm thermowells located in the center of the 4 mm diameter solid bed. The measured temperature in the thermowell was 945 K at the end of the synthesis with the furnace controlled at 980 K. Temperature differences were smaller at lower temperatures. It should be emphasized that this temperature represents an average temperature measured in a nonisothermal bed.

N_2 formation data from Fig. 1 were used to calculate first order and zero order Tamaru rate constants used in Arrhenius-type plots (Figs. 2, 3). Test plots assuming Temkin-Pyzhev type kinetics ($\alpha = 0.4$) were highly nonlinear. First order and zero order plots are linear in the lower temperature ranges but deviate from linearity at higher furnace temperatures due to hindered heat transfer in the bed, as observed experimentally. The measured furnace temperature is not the same as the actual bed temperature. For this reason, the Arrhenius expressions for the intrinsic rate constants were obtained using only the low temperature data:

$$k^0 = 2.554 \times 10^{11} \exp(-16{,}702/T) \quad \text{mol/s m}^3 \quad [6a]$$

$$k^1 = 3.462 \times 10^{10} \exp(-17{,}790/T) \quad \text{s}^{-1} \quad [6b]$$

Solid Structures

The Mo_2N sample used for the kinetic studies (above) was passivated by slow exposure to air at room temperature and removed for analysis. X-ray diffraction showed the presence of Mo_2N with no impurities. BET surface area of the passivated product was 80.0 m^2/g.

Solid intermediates in the NH_3/MoO_3 reaction were prepared by halting the temperature program at 473, 573, 673, 773, 873, and 980 K (zero dwell time). A relatively high NH_3 space velocity (ca. 100,000 hr^{-1}) and a constant temperature ramping rate of 0.01 K/sec were used for these syntheses. These conditions were chosen to dupli-

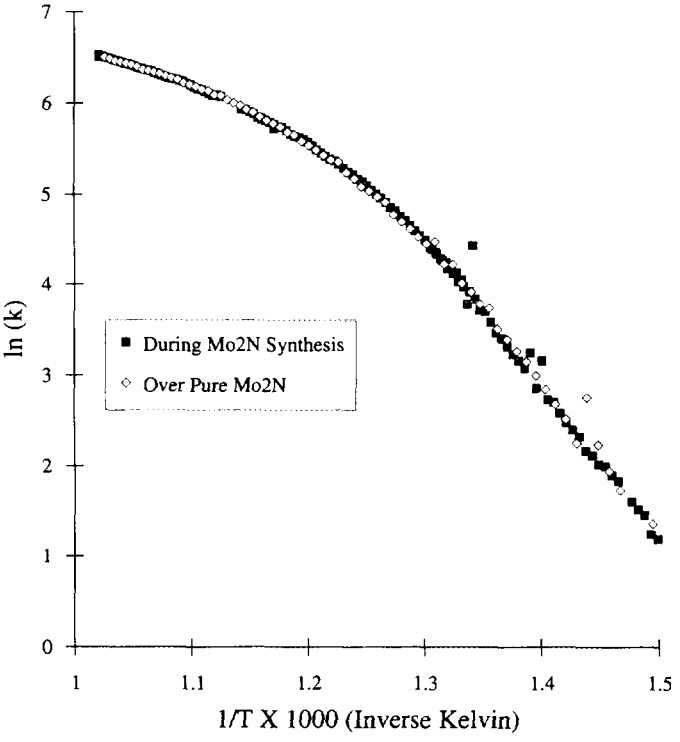

FIG. 3. Arrhenius plot for NH_3 decomposition reaction, zero order kinetics. Inverse furnace temperature is shown on the horizontal axis. Deviations from linearity at high temperature are due to differences between furnace and catalyst bed temperatures.

TABLE 1
Evolution of Solid State Structure During MoO_3/NH_3 Reaction

Sample	Temperature	Composition	Surface area
SYN0	298 K	MoO_3	2.7 m^2/g
SYN2	473 K	MoO_3	3.9 m^2/g
SYN3	573 K	MoO_3/unknown	3.9 m^2/g
SYN4	673 K	MoO_2/unknown	18.2 m^2/g
SYN5	773 K	MoO_2/γ-Mo_2N	24.9 m^2/g
SYN6	873 K	MoO_2/γ-Mo_2N	120 m^2/g
SYN7	980 K	MoO_2/γ-Mo_2N	97.0 m^2/g
SYN7 + 2	980 K + 2 hr	γ-Mo_2N	80.3 m^2/g

cate the best reported method for preparation to topotactic γ-Mo_2N (1, 2).

Sample compositions determined from X-ray diffraction data and BET surface areas of the intermediates are summarized in Table 1. The sharp X-ray diffraction pattern of polycrystalline MoO_3 is disrupted upon heating to 473 K, giving rise to a much noisier pattern in which MoO_3 is the predominant product, although some new reflections between 10 and 14° appear. At 573 K, MoO_3 is observed as well as an unknown peak corresponding to a lattice spacing of 804 pm. Peaks are also much broader than peaks in the starting material. At 673 K, no MoO_3 is present but MoO_2 is observed, as well as unknown peaks at 621, 307, and 205 pm. The signal/noise ratio is significantly lower. As the reaction proceeds to 773K and higher, Mo_2N peaks appear, which become broader with temperature. Relatively narrow MoO_2 peaks are also observed in the 773 and 873 K intermediates.

Scherrer analysis of the peak widths of the unknown compounds in the 573 and 673 K syntheses indicate that the unknown crystallites are larger than 1000 Å. Intermediate MoO_2 crystallites present in the 673, 773, 873, and 980 K syntheses are also larger than 1000 Å. The extent of the coherently diffracting domains in γ-Mo_2N, however, are of the order of 21 nm in the 773 K synthesis, and reach a minimum of ca. 9 nm at 873 K (Table 2). Mo_2N particle sizes increase as reaction progresses beyond 873 K. The minimum in Mo_2N particle size at 873 K corresponds to the maximum observed in specific surface area. Previous reports (1) indicated that a final furnace temperature of 980 K gave good results but acknowledged that the final reaction temperature was not necessarily optimized. Our data show that final furnace temperatures lower than 980 K give higher specific surface areas in our reactor configuration.

TABLE 2
Mo_2N Crystallite Size Determined Using X-Ray Linewidth and Surface Area Data

Sample	Temperature	D_{hkl}	D_p
SYN5	773 K	20.7 nm (111)	30.3 nm
SYN6	873 K	13.3 nm (111) 8.97 nm (200)	5.3 nm
SYN7	980 K	12.6 nm (111) 10.8 nm (200)	6.5 nm
SYN7 + 2	980 K + 2 hr	15.0 nm (111) 14.6 nm (200)	7.9 nm

Bed Temperature Calculations

At higher furnace temperatures (nonisothermal regimes), bed temperatures in the small (0.1 g) solid bed were calculated by simultaneous solution of 2-dimensional (r, z) heat and mass transfer equations. A two-dimensional continuum model was developed and solved numerically using Crank–Nicholson methods. Equations (6a) and (6b) were input to model rates of endothermic reaction. All of the required transport properties and thermodynamic data were known except the effective thermal conductivity of the solid bed. The effective thermal conductivity lumps the effects of convection and conduction into one parameter (23). A value of 1 cal/m sec K was assumed based on values observed in similar systems of metallic particles (23). Temperature-dependent enthalpy of reaction terms based on the experimentally determined kinetic expressions were also used in these calculations. The total enthalpy changes associated with the gas/solid reaction were much smaller than the enthalpy changes associated with decomposition of the rapidly flowing ammonia and thus were not included in the model. The effects of intraparticle heat and mass transfer (9) were found to be negligible in this bed of small (<20 μm) particles.

Development of boundary conditions required a careful analysis of heat transfer from the furnace to the outer surface of the bed. Natural convection from the heated air in the oven (where the furnace thermocouple was located) to the quartz tube was approximated by $Nu_D = 0.125\ Ra_D^{0.333}$, as suggested by Morgan (24) for Rayleigh numbers in the range of 10^7 to 10^{12}. The temperature dependence of thermal conductivity of the fused quartz tube was included in the model, as were temperature dependencies of all fluid properties. The heat transfer coefficient from the wall to the fixed bed/reactant gas mixture was estimated using a correlation from Jakob (25),

$$\frac{h_w D_T}{K_g} = Cf^* D_T^{0.17} \left(\frac{D_p G}{m}\right)^{0.83} N\mathrm{Pr}, \qquad [7]$$

where f^* is a function of D_p/D_T and C is used to correct from the given English units to SI. The effects of radiation from the furnace surface to the reactor were also included in the description of heat transfer from the furnace to the catalyst bed (9).

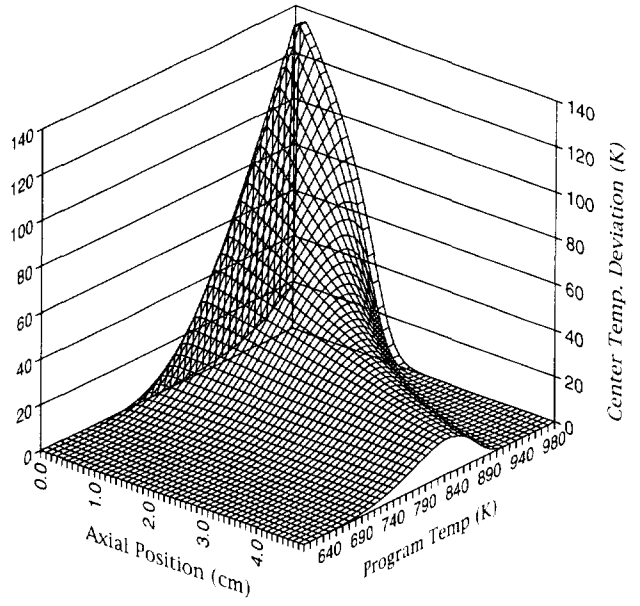

FIG. 4. Deviation of the centerline temperatures from the program (furnace) temperatures during temperature programmed reaction (small bed).

The temperatures of the bed were found to differ significantly from the temperature of the furnace at higher furnace temperatures, especially near the leading edge of the bed (Fig. 4). Axial and radial temperature gradients were found to exist inside the bed as well as temperature gradients between the outside surface of the bed and the furnace (Figs. 4, 5). The magnitude of the gradients increased with furnace temperature. Centerline temperatures as much as 120 K lower than the furnace temperature are observed. Radial temperature differences as large as 80 K are calculated, indicating that the surface temperature of the bed can be as much as 40 K lower than the temperature of the furnace. These calculated values agree reasonably well with the 35 K bed temperature depression measured experimentally using a thermowell. While the measured value is somewhat smaller than calculated, these values are not expected to match because the relatively large thermowell intrudes into the bed, displacing a large portion of catalyst. Smaller temperature differences result from the displacement of catalyst.

The outlet "mixing cup" composition was also determined in the heat and mass transfer model. Calculated values of outlet composition from the first order kinetic model compared quite well with those measured experimentally. The assumed value of bed thermal conductivity (1.0 cal/m s K) was varied to obtain a best fit of the calculated and experimental outlet compositions (Fig. 6). A regressed effective thermal conductivity of 0.95 cal/m s K was obtained. Figure 6 indicates that the first order model fits the experimental data better than the zero order model. In addition, the model fits well over a wide range of reactor temperatures.

Calculated bed temperatures were used to determine the local temperature ramping rates in the reactant bed (Fig. 7). When the furnace is ramped at 0.6 K/min, the actual temperature ramp experienced at times by the reactants is as much as 1.2 K/min in some regions of the bed. This effect occurs because some regions of the bed are relatively cool due to the endothermic reactions, but as the furnace temperature increases, the reactions are completed upstream in the reactor, so these cooler regions warm more rapidly.

The above calculations are valid only for the small bed size used to obtain experimental data (4 mm diameter). In order to predict the operation of a reactor producing large amounts of Mo_2N, a similar model of a bed 50 cm diameter by 25 cm to be used to synthesize large amounts of Mo_2N powder was generated. The model shows (Fig. 8) that limited heat transfer makes large-scale synthesis difficult: a gradient of several hundred degrees exists inside the bed, making control of the bed temperature problematic.

DISCUSSION

Bed Temperature Modeling

The kinetic results and heat transfer model show that limited heat transfer in the solid bed can interfere with the

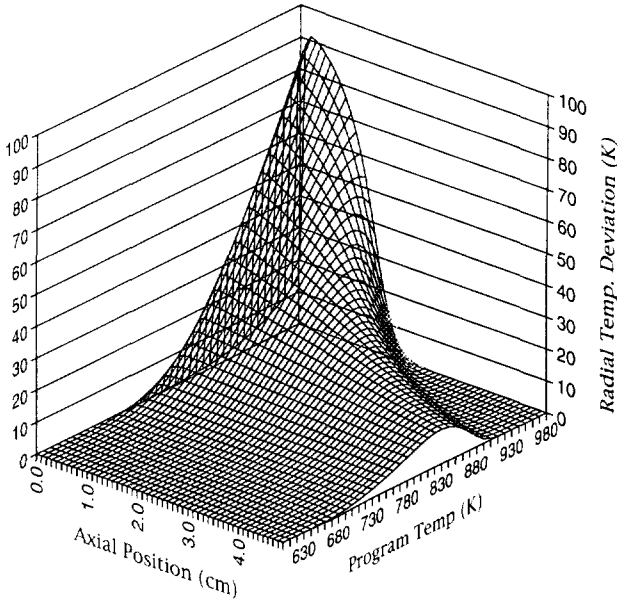

FIG. 5. Bed surface temperature minus centerline temperature during temperature programmed reaction (small bed).

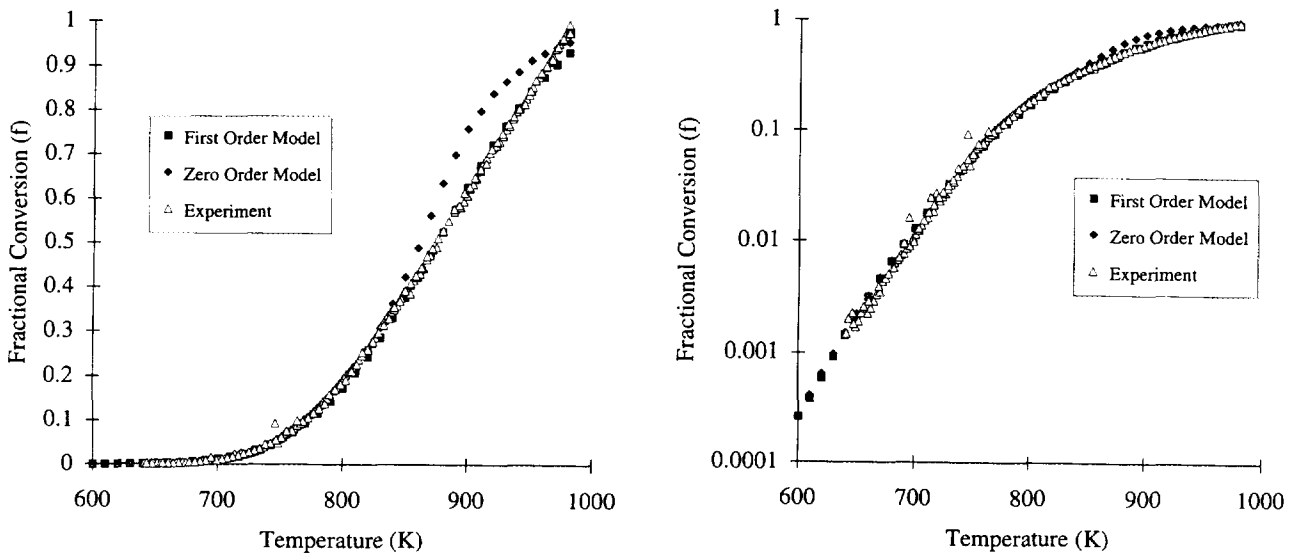

FIG. 6. Calculated and experimentally observed NH_3 conversions (linear and logarithmic plots provided for clarity).

endothermic temperature programmed reaction of MoO_3 and NH_3. The bed temperature is as much as 120 K cooler than the surrounding furnace in the small beds used in this study. Temperature gradients are even larger for larger beds. This effect is important because low final reaction temperatures result in incomplete reaction and low surface areas while high final reaction temperatures lead to product sintering. Thus, any complete specification of a NH_3/MoO_3 reaction temperature program reactions must recognize that the bed is not isothermal and that the optimum is valid only for specified bed dimensions and NH_3 flow rates. Placing the control thermocouple inside the bed would allow for more accurate temperature measurement, but gradients would still exist in the bed.

Another important effect of limited heat transfer is distorted local temperature ramping rates (Fig. 7). It has been shown (2) that ramping rates of 1 K/min and above

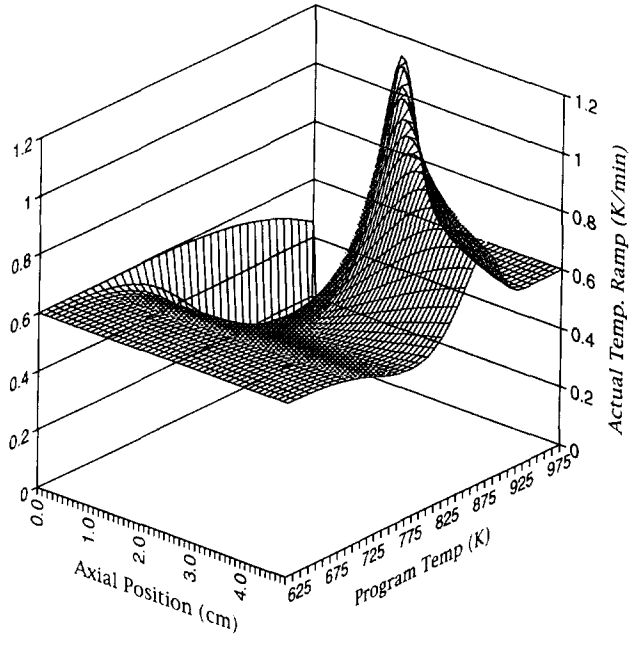

FIG. 7. Local temperature ramp observed along the centerline of the solid bed during temperature programmed reaction (small bed).

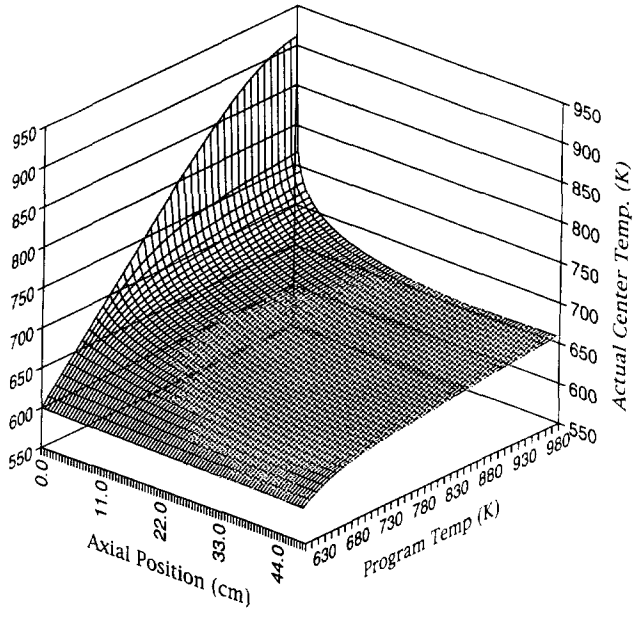

FIG. 8. Temperatures along centerline during temperature-programmed Mo_2N synthesis in a large bed.

lead to lower surface areas in NH_3 reactions as well as in N_2H_2 reactions in which ramping rate distortions are not expected. Thus, it is expected that some regions of the bed will yield lower surface area material due to the effects of heat transfer on the local temperature ramping rates.

While NH_3 decomposition can affect bed temperatures, the altered gas-phase chemistry does not catastrophically affect the generation of surface area. We have previously shown (8) that temperature-programmed reaction of MoO_3 and N_2/H_2 (in which bed temperature gradients are eliminated by elimination of the endothermic reaction) leads to high surface area Mo_2N with an optimum final reaction temperature located at 933 K. This value agrees well with the average calculated bed temperature when the furnace is at the final temperature of 980 K, the previously reported optimum for the NH_3/MoO_3 reaction (1). The highest surface areas we have achieved (up to 160 m^2/g, passivated) were obtained in reactions using N_2/H_2 mixtures with traces of NH_3, probably because of the precise temperature control which is possible using N_2/H_2 mixtures. The efficacy of N_2/H_2 is surprising because studies of molybdenum metal nitriding (26–30) report that NH_3 is a much more rapid nitriding agent than N_2, consistent with the low bond dissociation energies of NH_3 relative to triply bound N_2 (31). Our results show that high surface area is achieved using either NH_3 or N_2/H_2 mixtures.

The effects of limited heat transfer on large beds were shown to be great. The effect of bed volume on bed temperatures and sintering provides an explanation for the failure of previous large-scale syntheses to produce high specific surface area γ-Mo_2N (3). With bed gradients of 250 K in our large-scale model bed, it is not possible to heat the center of the bed to reaction temperature without overheating the outside of the bed to sintering temperatures. For this reason, it is not possible to produce large quantities of high-surface area Mo_2N using temperature-programmed reaction of NH_3 and MoO_3 without addressing the heat transfer problems. We propose an alternative synthesis method which eliminates heat transfer problems by using N_2/H_2 mixtures, perhaps with small amounts of added NH_3. The altered gas-phase chemistry does not alter the chemical composition of the final product.

NH_3 Decomposition Kinetics

While no previous reports of the kinetics of catalytic NH_3 decomposition by Mo_2N in this range of temperatures and pressures are available, Oyama has reported data for decomposition by VN under virtually identical conditions (13). The specific rate of decomposition (μmol/$s \cdot m^2$) at 800 K is 20.2 times more rapid over Mo_2N than over VN at 1 atm. Oyama observed a transition between the Temkin–Pyzhev and Tamaru mechanisms at 750 K using 20.0 m^2/g VN beds. The transition between mechanisms produces Arrhenius plots with two different linear regions very similar to those observed in the present work. Over VN, the reaction rate in the high temperature (Tamaru) region is limited by the kinetics of NH_3 adsorption. Over Mo_2N, the reaction rate at high temperature is limited, at least in part, by hindered heat transfer. Direct temperature measurements (using a thermowell) and heat transfer modeling provide evidence of this temperature aliasing effect. Hindered heat transfer is not expected to affect the VN results because of the lower specific rate of reaction and the lower catalyst surface area.

The pseudo-first order Tamaru mechanism fits the experimental data well. The Temkin–Pyzhev rate equation includes a strong inverse dependence on the partial pressure of hydrogen, which was not observed. However, a detailed study of decomposition reaction kinetics using a range of feed compositions (including different P_{H_2}, P_{N_2}, and P_{NH_3}) was not performed. All kinetic equations with orders between 0 and 1 predict large temperature gradients.

The apparent coincidence of the decomposition rates during Mo_2N synthesis and that over pure Mo_2N is interesting. Small but measurable differences in the amounts of N_2 observed in the effluent exist at lower temperatures and are due to consumption of nitrogen by the Mo_2N synthesis reaction. In the temperature ranges where NH_3 decomposition rates were measured, the Mo_2N synthesis reaction and generation of surface area is partially completed. It is possible the catalytically active surface phase at this point during temperature programmed reaction is similar to that of the final product.

Differences between Mo_2N particles sizes calculated from X-ray linewidths and from surface area data are due primarily to the presence of amorphous material and, to a lesser extent, of MoO_2. Particle size values would match if each sample consisted of only crystalline spherical Mo_2N particles. Small amounts of unreacted MoO_2 are present in all samples except SYN7 + 2, but the small amount of MoO_2 present cannot account for all of the observed differences. Therefore, nonspherical or amorphous aberrations must account for the observed differences. Our recent scanning tunnelling microscopy work has shown the samples consists of an aggregation of rounded particles. Therefore, the observed differences are due to the presence of amorphous material.

CONCLUSIONS

NH_3 was shown to decompose over high surface area Mo_2N and during temperature programmed synthesis of Mo_2N. Kinetic data fit a first order Tamaru rate expression

with an activation energy of 35.35 kcal/mol. Models of the bed during temperature programmed Mo_2N synthesis show that the endothermic NH_3 decomposition reaction interferes with the temperature program, resulting in lower than expected bed temperatures and distorted local temperature ramps. The effect is magnified in large beds, making large-scale syntheses difficult. It is proposed that an improved method for the large-scale synthesis of high-surface area Mo_2N synthesis would replace NH_3 with N_2/H_2 mixtures.

ACKNOWLEDGMENTS

This work was supported by the College of Engineering and the Department of Chemical Engineering at the University of South Carolina. One of us (RSW) thanks the Carolina Eastman Company for a graduate research fellowship.

REFERENCES

1. Volpe, L., and Boudart, M., *J. Solid State Chem.* **59,** 332 (1985).
2. Markel, E. J., and Van Zee, J. W., *J. Catal.* **126,** 643 (1990).
3. Oyama, S. T., Schlatter, J. C., Metcalf, J. E., and Lambert, J. M., *Ind. Eng. Chem. Res.* **27,** 1639 (1988).
4. Volpe L., and Boudart, M., *J. Phys. Chem.* **90,** 4878 (1986).
5. Ranhotra, G. S., Bell, A. T., and Reimer, J. A., *J. Catal.* **108,** 40 (1987).
6. Schlatter, J. C., Oyama, S. T., Metcalf, J. E., and Lambert, J. M., *Ind. Eng. Chem. Res.* **27,** 1648 (1988).
7. Oyama, S. T., and Sajkowski, D. J., *Prepr. Am. Chem. Soc. Div. Pet. Chem.* **35** (2), 233 (1990).
8. Wise, R. S., and Markel, E. J., *J. Catal.* **145,** 344 (1994).
9. Wise, R. S. Master's Thesis. University of South Carolina, 1992.
10. Bare, S. R., Strongin, D. R., and Somorjai, G. A., *J. Phys. Chem.* **90,** 4726 (1986).
11. Boudart, M., *Catal. Rev.—Sci. Eng.* **23,** 1 (1981).
12. Ozaki, A., and Aika, K. *in* "Catalysis, Science and Technology" (J. R. Anderson and M. Boudart, Eds.), Vol. 1, p. 87. Springer-Verlag, Berlin, 1981.
13. Shindo, H., Egawa, C., Inishi, T., and Tamaru, K., *J. Chem. Soc. Faraday Trans. I* **76,** 280 (1980).
14. Boudart, M., Egawa, C., Oyama, S. T., and Tamaru, K., *J. Chim. Phys.* **78,** 987 (1981).
15. Löffler, D. G., and Schmidt, L. D., *J. Catal.* **44,** 244 (1976).
16. Löffler, D. G., and Schmidt, L. D., *J. Catal.* **41,** 440 (1976).
17. Tamaru, K., *Acc. Chem. Res.* **21,** 88 (1988).
18. Temkin, M. I., and Pyzhev, V., *Acta Physicochim. USSR* **12,** 217 (1940).
19. Oyama, S. T., *J. Catal.* **133,** 358 (1992).
20. Wise, R. S., and Markel, E. J., unpublished results.
21. McClune, W. F., (Ed.), JCPDS Powder Diffraction File (Inorganic), 1985.
22. Klug, H. P., and Alexander, L. E., "X-Ray Diffraction Procedures," Chap. 9. Wiley, New York, 1962.
23. Kunii, D., and Smith, J. M., *AIChE J.* **6,** 71 (1960).
24. Morgan, V. T., *in* "Advances in Heat Transfer" (T. F. Irvine and J. P. Hartnett, Eds.), Vol. II, p. 199. Academic Press, New York, 1975.
25. Klug, H. P., "CRC Handbook of Chemistry and Physics." CRC Press, Ann Arbor, MI, 1990.
26. Cendlewska, B., Morawski, A., and Misiuk, A., *J. Phys. F. Met. Phys.* **17,** L71 (1987).
27. Saur, E. J., Schlechinger, H. D., and Rinderer, L. *IEEE Trans. Magnetics* **17** (1), 1029 (1981).
28. Brauer, G., and Leibbrandt, F., *J. Less-Common Met.* **12,** 57 (1967).
29. Jung, J., Morawski, A., and Karpinski, J., *Physica* **139,** 639 (1986).
30. Schoenberg, N., *Acta Chem. Scand.* **8,** 204 (1954).
31. Sharpe, A. G., "Inorganic Chemistry," Longmans, London, 1981.